16th World Conference on Earthquake, 16WCEE 2017

Santiago Chile, January 9th to 13th 2017

Paper N° 3136

Registration Code: S-X1461795378

MODIFICATION OF EXISTING MODELS TO INCLUDE THE EFFECT OF ROTATION ON THE BEHAVIOR OF ELASTOMERIC BEARINGS

S. Rastgoo Moghadam(1), D. Konstantinidis(2)

(1) *PhD Candidate, McMaster University, rastgos@mcmaster.ca*
(2) *Assistant Professor, McMaster University, konstant@mcmaster.ca*

Abstract

Seismic isolation is a design approach that aims at reducing earthquake demands on a structure and its contents. Conventional practice places the isolation system at the foundation level and calls for the construction of rigid diaphragms above and below the isolation layer. Consequently, these rigid diaphragms prevent the isolators from experiencing rotation, and the isolators displace horizontally and vertically only. However, there are several scenarios where isolators do experience rotations, including in tall buildings, in mid-story isolation applications, in bridges, etc. Various mechanical models have been proposed to investigate the horizontal behavior of elastomeric isolators under the assumption of zero top and bottom rotation. Those studies have characterized the effect of vertical load on the lateral stiffness and the lateral stability limit (defined as the displacement at which the tangent stiffness becomes zero). In this study, three existing models are considered: the Nagarajiah-Ferrell, Iizuka, and Han-Warn models. First, these three models are evaluated by comparing their predictions to results of Finite Element Analysis (FEA), assuming no rotation at the supports. Then, the models are modified to account for the effect of rotation. The modified models are evaluated using results from FEA under prescribed rotation values. The results show that the Han-Warn model provides more accurate predictions than the Nagarajiah-Ferrell and Iizuka models.

Keywords: elastomeric bearing; rubber bearing; rotation

1. Introduction

Seismic isolation is an approach to earthquake resistant design that aims at decreasing the seismic demand rather than increasing the structure's seismic capacity [1]. This is achieved through the introduction of a horizontally flexible layer that in effect decouples the superstructure from the horizontal seismic excitation. The most widely used seismic isolation devices for buildings and bridges are steel-reinforced elastomeric bearings. These bearings are made of layers of natural or synthetic rubber, often filled to enhanced their damping properties, interleaved with thin steel reinforcing plates (shims). A typical elastomeric isolator features thick steel end plates, bonded to the rubber during the vulcanization process. The end plates are connected to the superstructure and substructure with bolts. The manufacturing process for elastomeric bearings has to be conducted precisely to provide an adequate bond between the rubber and the steel [2].

Past studies have shown that elastomeric isolators under combined axial and horizontal loading behave nonlinearly, and an individual isolator undergoing large lateral displacements may experience a decrease in its axial-load capacity [3]. Previous experimental and analytical studies assessed the horizontal behavior of elastomeric bearings under the assumption that the bearing was sheared and compressed but the top and bottom supports did not experience any rotation. This assumption is often fairly valid due to the high rigidity of structural elements above and below the bearing which prevent it from experiencing rotation at the supports. There are, however, several scenarios where it is possible for an isolator to experience rotation. Ohsaki, et al. [4] who investigated the dynamic response of a base-isolated 10-story reinforced concrete frame building using 3D FEA, noted that the elastomeric isolators experienced rotation at their supports. In applications such as isolation of high-rise buildings or mid-height isolation, the effect of rotation may be significant. The effect of rotation may also be important in bridge applications, where the seismic isolators are placed between the bridge deck and the piers or abutments can experience rotation due to flexure of the deck above the isolator or the piers below. Rastgoo Moghadam and Konstantinidis [5] who investigated the effect of rotation on the lateral behavior of elastomeric isolators using 3D FEA noted that rotation does not significantly affect the critical displacement at the instability point (i.e., the point at which the tangential lateral stiffness becomes zero) but can decrease or increase the critical shear force. It was concluded that rotation at the supports, depending on the rotation value and the axial force, can appreciably influence the lateral behavior of a rubber bearing, and consequently it cannot be neglected.

There are many experimental studies in the literature [6-12] focused on the horizontal behavior and instability (critical) point of bearings. Since this study focuses on mechanical models that are capable of estimating the critical point, the introduction briefly discusses models currently available in the literature. Koh and Kelly [13] proposed a simple two-spring mechanical model including both shear and flexural deformations, to study the stability of elastomeric isolators. They compared the results of this model with experimental results for natural rubber bearings; it was shown that the model captured the behavior with good accuracy. Koo, et al. [14] modified the Koh-Kelly model by using an instantaneous apparent shear modulus obtained from test results instead of a constant shear modulus value. In this model the shear modulus is a function of the shear strain and can be represented by a polynomial function obtained by least squares fitting of test results. Nagarajaiah and Ferrell [15] developed a nonlinear analytical model which is an extension of the Koh-Kelly model to include large displacements. They showed that the critical load and horizontal stiffness decreases with increasing lateral displacement. Iizuka [16] developed a model by introducing finite deformation and nonlinear springs into the Koh-Kelly model. Based on experimental and analytical results, this model accurately captures the characteristics of elastomeric bearings, such as hardening, load deterioration, and buckling phenomena. The nonlinear parameters of the rotational and shear springs in the model are determined through experimental testing. The advantage of this model is that it can easily handle a variable axial force. A three-dimensional model which includes multiple shear springs at the mid-height and a series of axial springs at the top and bottom of an isolator was proposed by Yamamoto, et al. [17] and Kikuchi, et al. [18] for circular and rectangular isolators, respectively. Han and Warn [19] conducted sensitivity analysis on previous models using FEA and proposed an alternative model which does not rely on experimentally calibrated parameters. This model includes a series of vertical springs with a simple bilinear constitutive relationship. These vertical springs replace the rotational spring which was used in the Koh-Kelly model. The solution process to find the critical point is similar to that in the Iizuka model. Vemuru et al. [20] showed that the Nagarajaiah-Ferrell model cannot accurately predict the stiffness degradation beyond the stability point. As this model is based on quasi-static tests, the stiffness of the bearings beyond the stability limit is larger than predicted by the model. Vemuru et al. [20] modified the Nagarajaiah-Ferrell model by incorporating higher order displacement terms in the rotational spring. The modified model is capable of characterizing the dynamic behavior of bearings more accurately than previous models, particularly beyond the instability point.

FEA is a common approach to understand the behavior of rubber isolators. Recently, studies using this approach have evaluated the behavior of isolation bearings under compression and shear [21-29]. Some FEA studies have focused specifically on the stability of bearings. Warn and Weisman [30] conducted a parametric study to investigate the effect of geometry on the critical load of rubber bearings using 2D FEA. Their results showed that the critical load is more sensitive to the bearing width and the individual rubber layer thickness than it is to the number of rubber layers. Montuori et al. [31] studied the effect of the second shape factor (defined as the ratio of the diameter/width to the total thickness of rubber material) on the stability of elastomeric bearings. They considered different bearings with a shape factor of 20 and a second shape factor ranging from 1.5 to 6.2. Their result showed that the lateral behavior and instability of the elastomeric bearings is related to the value of the second shape factor.

The objective of this paper is to evaluate and extend existing models available in the literature to capture the effect of rotation on the stability of elastomeric bearings. In this study, three models (Nagarajiah-Ferrell [15], Iizuka [16] and Han-Warn [19]) are considered. First, the paper summarizes these models and evaluates their performance by comparing their predictions to results of FEA assuming no rotation at the supports. Then, the models are extended to account for support rotation, and their predictions are compared against FEA under prescribed rotation values.

2. Review of Existing Mechanical Models

This section is intended to summarize the main equations of each model. For the specifics of each model discussed here, the reader is referred to the original paper.

The Nagarajaiah-Ferrell model (see Fig. 1a) is described the following nonlinear equations, which should be solved simultaneously [15]

$$u = s\cos\theta + h\sin\theta \tag{1}$$

$$v = s\sin\theta + h(1-\cos\theta) \tag{2}$$

$$M = K_\theta\,\theta = Pu + F(h-v) \tag{3}$$

$$Q_s = K_s\,s = P\sin\theta + F\cos\theta \tag{4}$$

where *h* is the total height of the bearing, s is the local shear deformation that develops in the linear shear spring with stiffness K_s, θ is the rotation concentrated in the rotational springs with the stiffness K_θ, *M* is rotational spring moment, and Q_s is the shear spring force. Under axial load *P* and shear force *F*, the model introduces the global horizontal displacement *u* and vertical displacement *v*. K_s and K_θ are obtained by Eqs. (5) and (6),

$$K_s = \frac{GA_s}{h}\left(1-0.325\tanh\left(\frac{s}{25.4}\right)\right) \tag{5}$$

$$K_\theta = \frac{\pi^2 EI_s}{h}\left(1-\left(\frac{25.4-t}{D}\right)\left(\frac{s}{25.4}\right)\right) \tag{6}$$

where *G* is the shear modulus of the rubber material, $A_s = A(h/t_r)$, A is the total cross sectional area, t_r is the total height of rubber, $EI_s = E_b I(h/t_r)$, E_b is the bending modulus of the elastomeric bearing, which is equal to $E_c/3$ for a circular baring, E_c is compression modulus, *S* is the shape factor, *I* is area moment of inertia of the rubber layer, t is the thickness of single rubber layer and D is the bearing diameter. For a circular bearing: $E_c = 6GS^2$, $S = D/4t$ and $I = \pi D^4 / 64$. It should be noted that s, t and D in Eqs (5) and (6) are in mm.

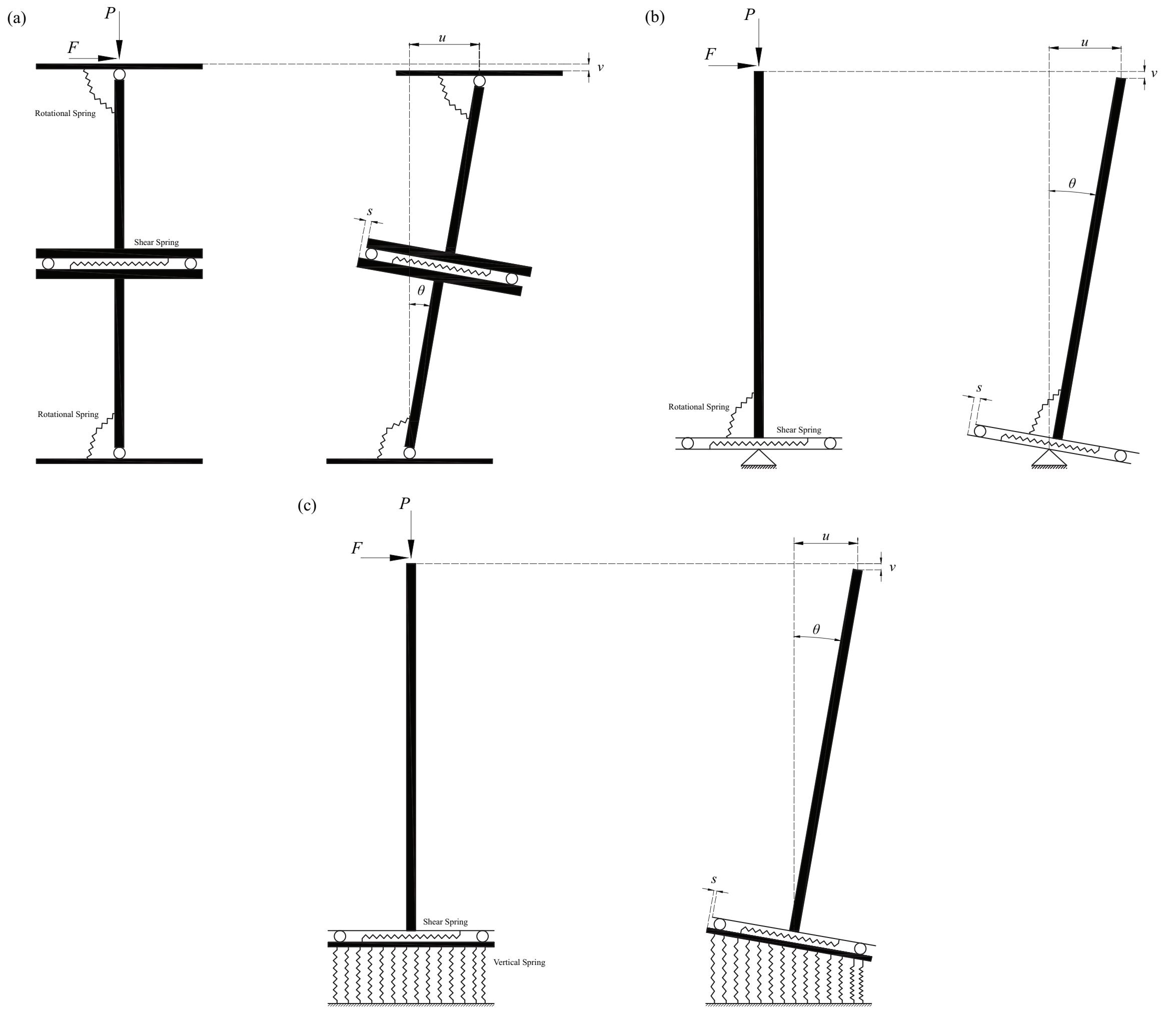

Fig. 1: Illustration of the mechanical models in the laterally unreformed and deformed shape: a) Nagarajiah-Ferrell b) Iizuka c) Han-Warn

Iizuka (see Fig. 1b) converted Eqs. (1)-(4) to finite difference format, from which Eq. (7) can be obtained [16],

$$\begin{bmatrix} {}_i(\Delta\theta) \\ {}_i(\Delta s) \\ {}_i(\Delta v) \\ {}_i(\Delta F) \end{bmatrix} = \begin{bmatrix} h\sin_i\theta + {}_is\cos_i\theta & \sin_i\theta & -1 & 0 \\ h\cos_i\theta - {}_is\sin_i\theta & \cos_i\theta & 0 & 0 \\ {}_i\left(\dfrac{dM}{d\theta}\right) & 0 & {}_iF & {}_iv - h \\ P\cos_i\theta - {}_iF\sin_i\theta & -{}_i\left(\dfrac{dQ_s}{d\theta}\right) & 0 & \cos_i\theta \end{bmatrix}^{-1} \begin{bmatrix} 0 \\ 1 \\ P \\ 0 \end{bmatrix} \Delta u \qquad (7)$$

where $\Delta\theta$, Δs, Δv and ΔF are the incremental response quantities for a given bearing, under the axial force, P, and incremental lateral displacement, Δu, at step i. They are added to the current step to find the response values at the next step (i+1), and this procedure is repeated until the critical point is obtained. In order to avoid ill-conditioned matrix, (to solve Eq. 7) linear spring properties can be assumed for the first step. The tangential rotational stiffness, $dM/d\theta$, and tangential shear stiffness, dQ_s/ds, at each step, can be obtained using

$$\frac{dM}{d\theta}=\begin{cases}\dfrac{\pi^2 EI_s}{h} & \left(\theta\le\theta_y\right)\\ \dfrac{\pi^2 EI_s/h}{\left[1+\dfrac{r}{3}\left(\dfrac{\theta}{\theta_y}-1\right)\right]^{(1+r/r)}} & \left(\theta>\theta_y\right)\end{cases} \tag{8}$$

$$\frac{dQ_s}{d\theta}=\frac{GA_s}{h}\left[1+s_1\left(1+s_2\right)\left(\frac{s}{t_r}\right)^{s_2}\right] \tag{9}$$

where r is a dimensionless parameter with a recommended value between 1.2 and 3.5. s_1 and s_2 are dimensionless parameters. s_1 can be varied between 0.0068 and 0.01 and s_2 is equal to 3. In this study $s_1=0.01$, $s_2=3$ and r = 2. θ_y is yielding rotational angle which is given by

$$\theta_y=\frac{2hZ\left(\sigma_y-\sigma\right)}{\pi^2 EI_s} \tag{10}$$

where Z is the elastic section modulus of bonded rubber area (=$\pi D^3/32$ for a circular bearing), σ is nominal stress (=P/A), and σ_y is the yielding stress, which is equal to 3G.

In the Han-Warn model (see Fig. 1c), the rotational spring is replaced by a series of parallel vertical springs. The cross section is discretized into individual springs, which is similar to a fiber-element model. The number of springs, n, should be large enough to obtain a converged solution for all axial loads for a given bearing. Similar to the Iizuka model, Eq. (7) is used. $dM/d\theta$ at each step is obtained by

$${}_i\left(\frac{dM}{d\theta}\right)=\frac{{}_iM-{}_{i-1}M}{{}_i\theta-{}_{i-1}\theta} \tag{11}$$

At each step, the vertical springs should satisfy

$$P=\sum_j^n \sigma_{s_j}A_j \tag{12}$$

$${}_iM=\sum_j^n \sigma_{s_j}A_j\left(d_{s_j}+x\right) \tag{13}$$

$$\frac{\varepsilon_{s_1}l_s}{d_{s_1}+x}=\frac{\varepsilon_{s_2}l_s}{d_{s_2}+x}=\dots=\frac{\varepsilon_{s_j}l_s}{d_{s_j}+x}=\dots=\frac{\varepsilon_{s_n}l_s}{d_{s_n}+x}=\theta \tag{14}$$

where σ_{s_j} and ε_{s_j} are the stress and strain in the jth vertical spring, respectively. σ_{s_j} can be determined from

$$\sigma_{s_j}=\begin{cases}E_c\varepsilon_{s_j} & \left(\varepsilon_{s_j}\le\sigma_y/E_c\right)\\ \sigma_y & \left(\varepsilon_{s_j}>\sigma_y/E_c\right)\end{cases} \tag{15}$$

where A_j is the area of the jth vertical spring element, d_{s_j} is the distance between the centre of the jth vertical spring and the center of the bearing cross section, x is the distance between the neutral axis and the center of the bearing cross section, and l_s is the initial length of vertical spring element which is calculated by

$$\frac{E_c}{l_s}\sum_j^n A_j d_{s_j}^2 = \frac{\pi^2 E_b I}{t_r} \tag{16}$$

The tangential shear stiffness, dQ_s/ds, is obtained by

$$\frac{dQ_s}{ds} = \frac{GA_s}{h}\left(1 - C_s \tanh\left(\frac{u}{t_r}\right)\right) \tag{17}$$

3. Evaluation of Existing Mechanical Models

In this study the mechanical models discussed in the previous section, are compared against FEA results for a given bearing. The detail of FEA model for three-dimensional circular bearings is available in [5]. Table 1 shows the properties of the bearing that is used in this study. This bearing is similar to the bearing tested by Weisman and Warn [11]. In this study, the compressible Neo-Hookean hyperelastic material model was used to describe the rubber material. This material model is defined by two material constants: the shear modulus *G* and the bulk modulus *K*. The strain energy function of the compressible Neo-Hookean model is [32],

$$W = C_{10}\left(\bar{I}_1 - 3\right) + \frac{1}{D_1}\left(J - 1\right)^2 \tag{18}$$

where $C_{10} = G/2$, $D_1 = 2/K$, $\bar{I}_1$ is the first reduced invariant (deviatoric part only) of the left Cauchy-Green deformation tensor, and J is the elastic volume ratio. The material parameter D_1 is 2×10^{-6} mm^2/N assuming incompressible material. The steel material was modeled using a bilinear isotropic material model with Young's modulus of 200 GPa and a Poisson's ratio of 0.3. A post-yield modulus of 2 percent of the initial modulus was specified.

Table 1: Properties of bearings used in this study

Properties	Symbol	Unit	
Outside diameter	D	mm	152
Thickness of individual rubber layer	t	mm	3
Thickness of individual steel shim	t_s	mm	3
Number of rubber layers	n_r	-	20
Shape factor	S	-	12.67
Second shape factor	S_2	-	2.53
Shear modulus	G	MPa	0.9

In the FEA model, all nodes of the top end plate were constrained to a point (control node) located at the centroid of the end plate. The boundary conditions were assigned to this point. The control node is free to move vertically and laterally in one direction and in the case of rotation; this node can rotate in the specified direction. Similar to the top end plate, all nodes at the bottom end plate were constrained to a control node. This point is restrained in all degrees of freedom except for the case of rotation. The analysis was performed in two stages: during the first stage, the axial load but also rotations were imposed gradually until the desired values were reached; and in the second stage of the analysis, the horizontal displacement is gradually increased while maintaining the axial load and rotation value from the first stage constant. The analysis includes nonlinear geometry, large displacements, and large strains. The incremental nonlinear analysis was conducted using an updated Lagrangian formulation and the Newton-Raphson iteration method.

To obtain the critical point, the constant axial force method [11] was used. In this method, which was experimentally confirmed by Sanchez et al. [12], the lateral displacement and shear force associated with the critical point are determined from the shear force-lateral displacement curve for a given constant axial load, *P*. In the loading part (FEA model), the axial load was applied first, and then the horizontal displacement was applied incrementally until the horizontal stiffness became zero and the shear force reached its maximum value.

In order to extend the Nagarajiah-Ferrell model to account for top support rotation, Eqs. (1) to (4) are modified by replacing θ by $\theta - \theta_t$. θ_t is the applied rotation at the top end plate, which is positive if the applied rotation is counterclockwise. To modify the Iizuka and Han-Warn models, the applied rotation θ_t is included in the linear spring properties in the first step.

3.1 Results under zero rotation of the top surface

Fig. 2 shows the lateral behavior of the bearing under different average pressure values, $\bar{p} = P/A = 5.5$, 8.26 and 11.02 MPa, as predicted using the three mechanical models and the FEA. As can be seen, the Han-Warn model results is in good agreement with the FEA results, especially for the common pressure (around 8 MPa) used in practical design. In all three cases, the Nagarajaiah-Ferrell model underpredicts the shear force F, while the Iizuka model overpredicts it, compared to the FEA results. A load-displacement curve, like the ones presented in Fig. 2, can be used to extract the u_{cr} and F_{cr} values that correspond to P_{cr}. From this information, Fig. 3 can be generated. The figure shows that the analytical models are in good agreement with the FEA results in terms of predicting the critical displacement, while there is a significant difference between the models in estimating the critical shear force. Predictions of the Han-Warn model and Iizuka models are close to each other, with the Iizuka model giving slighly larger values. Figs. 2 and 3 show that, in general, the Nagarajaiah-Ferrell model underestimates the shear force at the critical point, while the Iizuka model overestimates it.

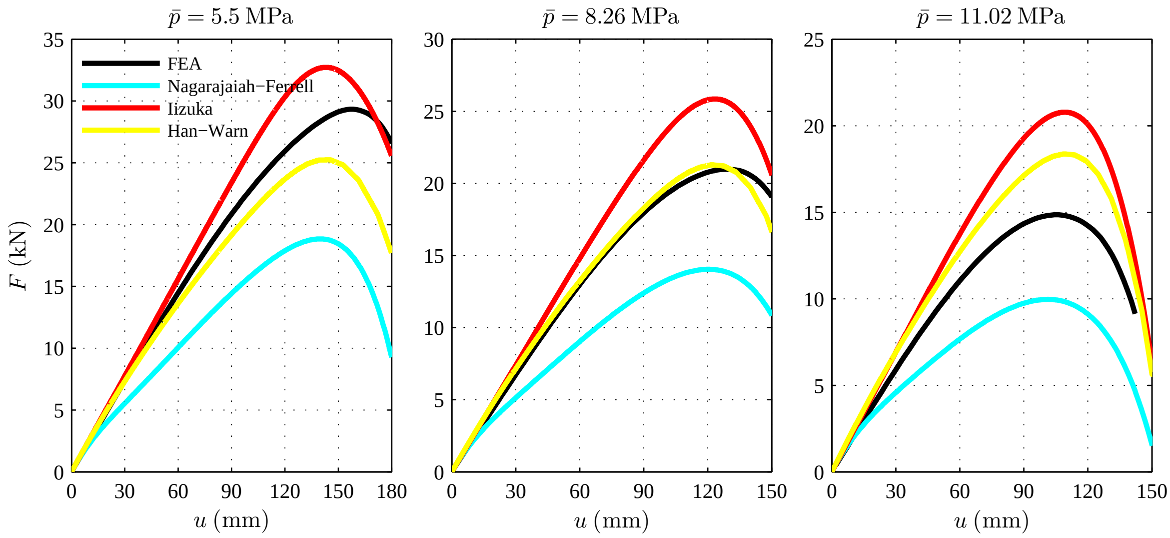

Fig. 2: Comparison of shear force-lateral displacement relationships obtained from the analytical models (Nagarajiah-Ferrell, Iizuka, and Han-Warn) and the FEA under average pressure of 5.5, 8.26 and 11.02 MPa

3.2 Results under rotation of the top surface

Fig. 4 shows the lateral behavior of the bearing under different average pressure values, $\bar{p} = 5.5$, 8.26 and 11.02 MPa, using modified analytical models to account for the effect of rotation, together with FEA results when the applied rotation at the top end plate is equal to 0.02 rad (left column) and 0.04 rad (right column). It shows that the Han-Warn model is in good agreement with the FEA results for both rotation values (0.02 and 0.04 rad), particularly for low and medium pressure values (5.5 and 8.26 MPa). In terms of initial state (force is not equal to zero at zero displacement) that shows the effect of rotation, all modified models overestimate the effect of rotation, particularly for the large pressure.

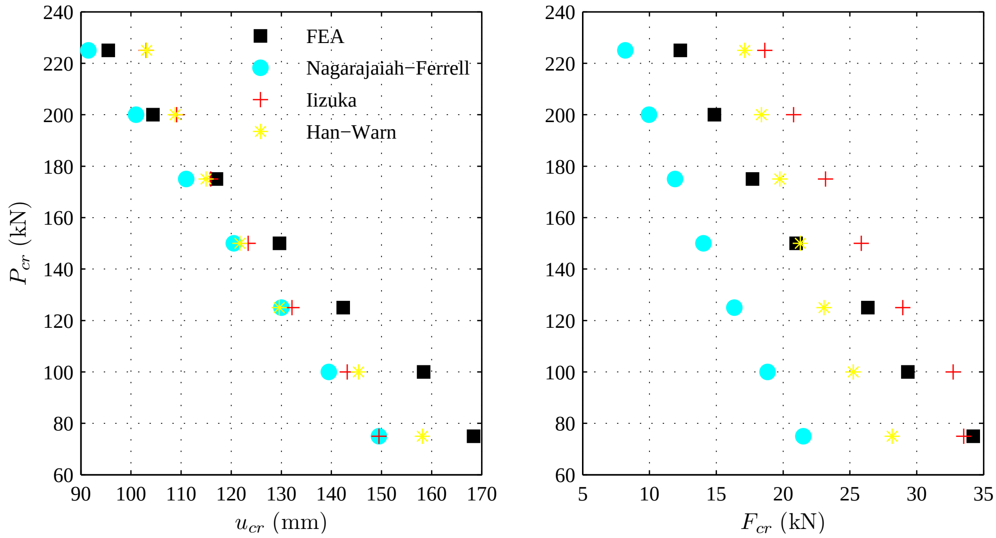

Fig. 3: Comparison of critical points predicted by the three analytical models (Nagarajiah-Ferrell, Iizuka, and Han-Warn) and the FEA

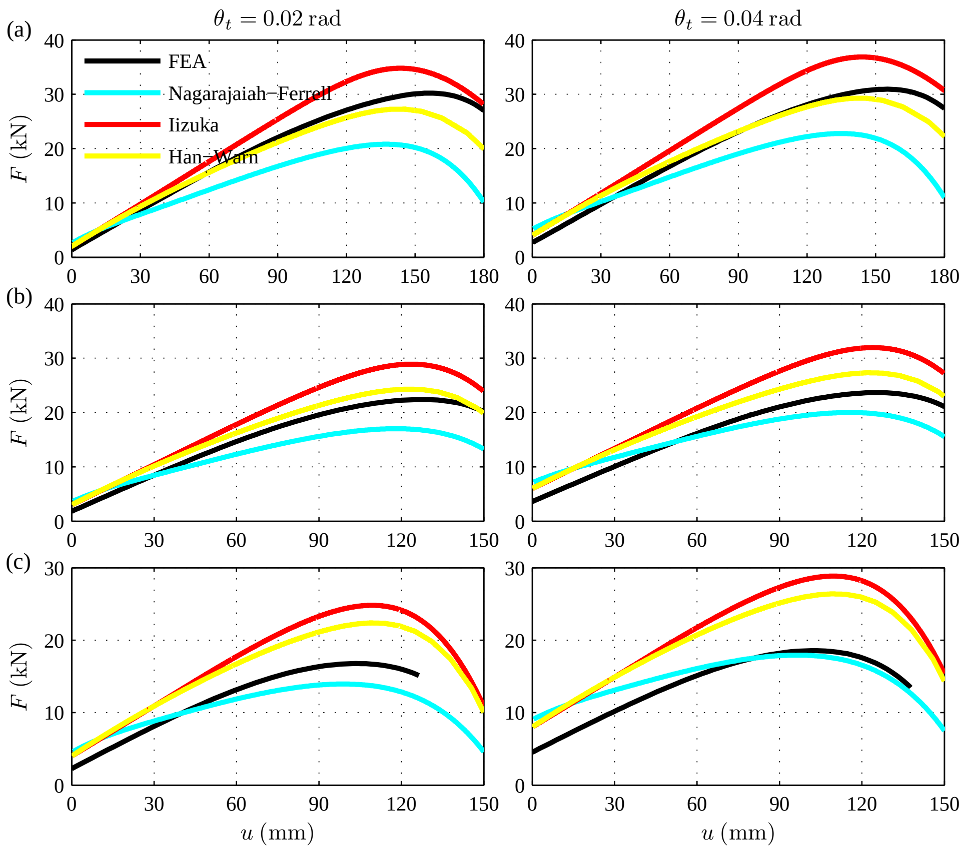

Figure 4: Comparison of shear force-lateral displacement relationships obtained using the modified analytical models (Nagarajiah-Ferrell, Iizuka, and Han-Warn) and the FEA under average pressure (a) 5.5 (b) 8.26 and (c) 11.02 MPa, and top rotation of $\theta_t = 0.02$ rad (left column) and $\theta_t = 0.04$ rad (right column)

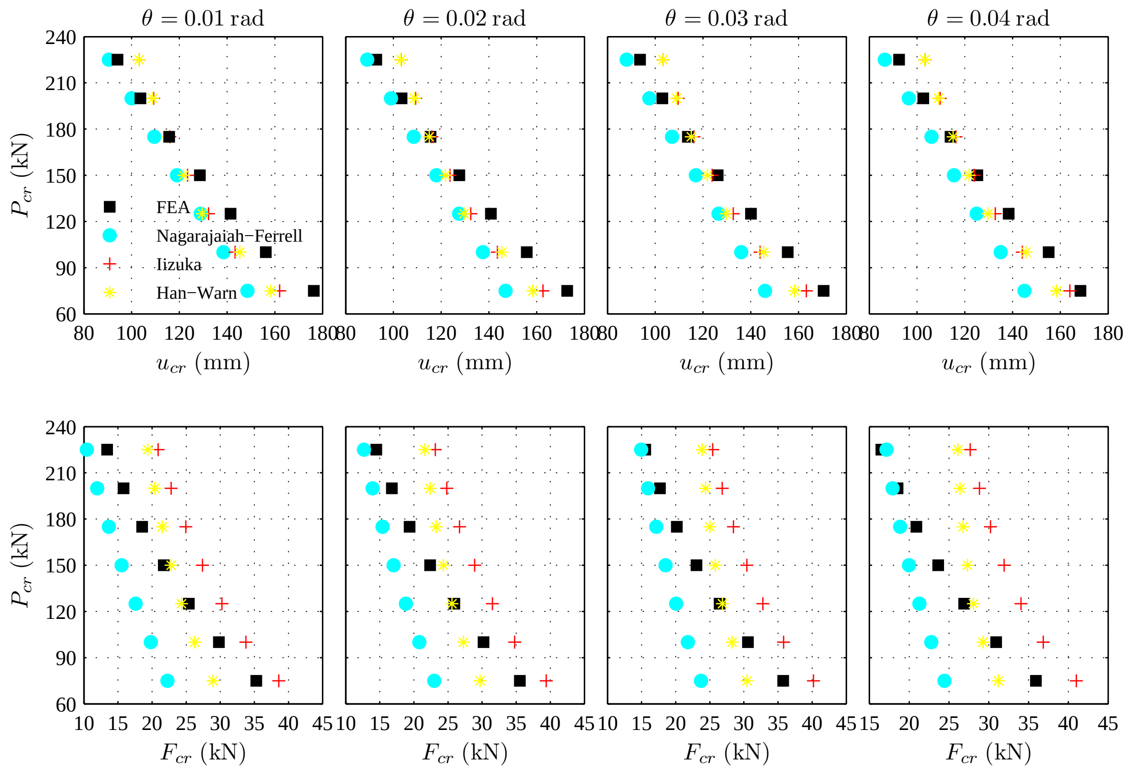

Figure 5: Comparison of critical points results between the modified analytical models (Nagarajiah-Ferrell, Iizuka, and Han-Warn) and Finite Element analysis ($\theta_t = 0.01$, 0.02, 0.03 and 0.04 rad)

Fig. 5 compares critical points as predicted by the modified analytical models and the FEA under different rotation values. Depending on the rotation value and pressure, critical forces vary significantly, but it can be seen that the larger value of pressure and rotation using modified analytical models cause larger error compared to the FEA results. Unlike the critical force, there is good agreement between the results for critical displacement. Yet, the agreement is more notable in lower value of rotation.

4. Conclusions

This paper considered three mechanical models, i.e., the Nagarajiah-Ferrell, the Iizuka, and the Han-Warn models, for assessing the stability of an elastomeric isolator. The study compared the results obtained using these models against FEA results for a given elastomeric isolation bearing, for the case of zero rotation at the top end plate and non-zero rotation at the end plates. The following summarizes the most important observation:

1. The Nagarajiah-Ferrell model, regardless of rotation value, predicts lower values of shear force at the critical point than the FEA. The relative difference becomes more significant for the bearing under larger value of pressure.
2. The Iizuka model overpredicts the shear force at the critical point.
3. The Han-Warn model provides better agreement with the FEA.
4. All models predict the displacement at the critical point with a good agreement with FEA.
5. All modified models overestimate the effect of rotation, particularly for the large pressure.

This study presented results for a given bearing, but to compare the results more comprehensively, more bearings, with a range of different properties, need to be analyzed. The authors are in the process of proposing a new model aimed at addressing the shortcomings of existing models.

5. Acknowledgements

The authors would like to gratefully acknowledge the financial support of the Natural Sciences and Engineering Research Council of Canada (NSERC).

6. References

[1] Naeim F, Kelly JM (1999): *Design of Seismic Isolated Structures: From Theory to Practice*. John Wiley & Sons.

[2] Kelly JM, Marsico MR (2010): Stability and post-buckling behavior in nonbolted elastomeric isolators. *Seismic Isolation and Protection Systems*, **1** (1), 41-54.

[3] Kelly JM, Konstantinidis D (2011): *Mechanics of Rubber Bearings for Seismic and Vibration Isolation*. Wiley.

[4] Ohsaki M, Miyamura T, Kohiyama M, Yamashita T, Yamamoto M, Nakamura N (2015): Finite-element analysis of laminated rubber bearing of building frame under seismic excitation. *Earthquake Engineering* & *Structural Dynamics*. **44** (11), 1881-1898.

[5] Rastgoo Moghadam S, Konstantinidis D (2015): Effect of rotation on the horizontal behavior of emastomeric isolators. *The 11th Canadian Conference on Earthquake Engineering*, Victoria, Canada.

[6] Buckle IG, Kelly JM (1986): Properties of slender elastomeric isolation bearings during shake table studies of a large-scale model bridge deck. *ACI Special Publication*, **94**.

[7] Aiken ID, Kelly JM, Tajirian FF (1989): Mechanics of low shape factor elastomeric seismic isolation bearings. *Technical Report PEER UCB/EERC-89/13*, Pacific Earthquake Engineering Research, Berkeley, USA.

[8] Buckle IG, Liu HK (1994): Experimental determination of critical loads of elastomeric isolators at high shear strain. *NCEER Bulletin*, **8** (3), 1-5.

[9] Buckle IF, Nagarajaiah S , Ferrell K (2002): Stability of elastomeric isolation bearings: experimental study. *Journal of Structural Engineering*, **128** (1), 3-11.

[10] Cardone D , Perrone G (2012): Critical load of slender elastomeric seismic isolators: an experimental perspective. *Engineering Structures*, **40**, 198-204.

[11] Weisman J, Warn GP (2012): Stability of elastomeric and lead-rubber seismic isolation bearings. *Journal of Structural Engineering*, **138** (2), 215-223.

[12] Sanchez J, Masroor A, Mosqueda G, Ryan K (2013): Static and dynamic stability of elastomeric bearings for seismic protection of structures. *Journal of Structural Engineering*, **139**, 1149-1159.

[13] Koh CG, Kelly JM (1988): A simple mechanical model for elastomeric bearings used in base isolation. *International journal of Mechanical Sciences*, **30** (12), 933-943.

[14] Koo GH, Lee JH, Yoo, Too B, Ohtori Y (1999): Evaluation of laminated rubber bearings for seismic isolation using modified macro-model with parameter equations of instantaneous apparent shear modulus. *Engineering structures*, **21** (7) 594-602.

[15] Nagarajaiah S, Ferrell K (1999): Stability of elastomeric seismic isolation bearings. *Journal of Structural Engineering*, **125** (9), 946-954.

[16] Iizuka M (2000): A macroscopic model for predicting large-deformation behaviors of laminated rubber bearings.

Engineering Structures. **22** (4), 323-334.

[17] Yamamoto S, Kikuchi , Ueda M, Aiken ID (2009): A mechanical model for elastomeric seismic isolation bearings including the influence of axial load. *Earthquake Engineering & Structural Dynamics*. **38** (2), 157-180.

[18] Kikuchi M, Nakamura T, Aiken ID (2010): Three-dimensional analysis for square seismic isolation bearings under large shear deformations and high axial loads. *Earthquake Engineering & Structural Dynamics*. **39** (13), 1513-1531.

[19] Han X, Warn GP (2014): Mechanistic model for simulating critical behavior in elastomeric bearings. *Journal of Structural Engineering*, **139** (12), 04013016.

[20] Vemuru VSM, Nagarajaiah S, Masroor A, Mosqueda G (2014): Dynamic lateral stability of elastomeric seismic isolation bearings. *Journal of structural engineering*, **140** (8) A4014014.

[21] Mordini A, Strauss A (2008): An innovative earthquake isolation system using fibre reinforced rubber bearings. *Engineering structures*, **30** (10), 2739-2751.

[22] Nguyen HH, Tassoulas JL (2009): Directional effects of shear combined with compression on bridge elastomeric bearings. *Journal of Bridge Engineering*, **15** (1), 73-80.

[23] Toopchi-Nezhad H, Tait MJ, Draysdale RG (2011): Bonded versus unbonded strip fiber reinforced elastomeric isolators: Finite element analysis. *Composite Structures*, **93** (2), 850-859.

[24] Osgooei PM, Tait MJ, Konstantinidis D (2014): Three-dimensional finite element analysis of circular fiber-reinforced elastomeric bearings under compression. *Composite Structures*, **108**, 191-204.

[25] Osgooei PM, Tait MJ, Konstantinidis D (2014): Finite element analysis of unbonded square fiber-reinforced elastomeric isolators (FREIs) under lateral loading in different directions. *Composite Structures*, **113**, 164-173.

[26] Van Engelen NC , Osgooei PM, Tait MJ, Konstantinidis D (2014): Experimental and finite element study on the compression properties of Modified Rectangular Fiber-Reinforced Elastomeric Isolators (MR-FREIs). *Engineering Structures*, **74**, 52-64.

[27] Rastgoo Moghadam S, Konstantinidis D (2014): The effect of slip on the compressive behavior of unbonded rubber pads: a Finite Element approach. *Proceedings of the 10th National Conference in Earthquake Engineering*, Earthquake Engineering Research Institute, Anchorage, USA.

[28] Osgooei PM, Van Engelen NC, Konstantinidis D, Tait MJ (2015): Experimental and finite element study on the lateral response of modified rectangular fiber-reinforced elastomeric isolators (MR-FREIs). *Engineering Structures*, **85**, 293-303.

[29] Konstantinidis D, Rastgoo Moghadam S (2016): Compression of unbonded rubber layers taking into account bulk compressibility and contact slip at the supports. *International Journal of Solids and Structures*, **87**, 206-221.

[30] Warn GP, Weisman J (2011): Parametric finite element investigation of the critical load capacity of elastomeric strip bearings. *Engineering Structures*, **33** (12), 3509-3515.

[31] Montuori GM, Mele E , Marrazzo G , Brandonisio G , De Luca A (2016): Stability issues and pressure-shear interaction in elastomeric bearings: the primary role of the secondary shape factor. *Bulletin of Earthquake Engineering*, **14**, 569-597.

[32] Bathe, K-J (1995): *Finite Element Procedures*, Prentice Hall.